The genetic basis of structural colour variation in mimetic *Heliconius* butterflies

Melanie N. Brien[1*], Juan Enciso Romero[1,2,*], Emma V. Curran[1], Andrew J. Parnell[3], Carlos Morochz[4], Patricio A. Salazar[1], Pasi Rastas[5], Thomas Zinn[6], Nicola J. Nadeau[1]

[1]Department of Animal and Plant Sciences, The University of Sheffield, Alfred Denny Building, Western Bank, Sheffield, S10 2TN, United Kingdom

[2]Biology Program, Faculty of Natural Sciences, Universidad del Rosario, Bogotá, Colombia

[3]Department of Physics and Astronomy, The University of Sheffield, Hicks Building, Hounsfield Road, Sheffield, S3 7RH, United Kingdom

[4]Biology & Research Department, Mashpi Lodge, Ecuador

[5]Institute of Biotechnology, University of Helsinki, Finland

[6]ESRF - The European Synchrotron, 38043, Grenoble Cedex 9, France

[*]These authors contributed equally. Correspondence: M. Brien (Current address: University of Jyväskylä, Finland, melanie.n.brien@jyu.fi) and J. Enciso Romero (juan.enciso@urosario.edu.co).

Short title: Structural colour genetics in *Heliconius* butterflies.

Keywords: Structural colour, iridescence, mimicry, *Heliconius,* QTL, convergence.

Abstract

Structural colours, produced by the reflection of light from ultrastructures, have evolved multiple times in butterflies. Unlike pigmentary colours and patterns, little is known about the genetic basis of these colours. Reflective structures on wing-scale ridges are responsible for iridescent structural colour in many butterflies, including the Müllerian mimics *Heliconius erato* and *Heliconius melpomene.* Here we quantify aspects of scale ultrastructure variation and colour in crosses between iridescent and non-iridescent subspecies of both of these species and perform quantitative trait locus (QTL) mapping. We show that iridescent structural colour has a complex genetic basis in both species, with offspring from crosses having wide variation in blue colour (both hue and brightness) and scale structure measurements. We detect two different genomic regions in each species that explain modest amounts of this variation, with a sex-linked QTL in *H. erato* but not *H. melpomene.* We also find differences between species in the relationships between structure and colour. Our results suggest that these species have followed different evolutionary trajectories in their convergent evolution of similar structural colour. This study provides a starting point for determining the genetic basis of structural colouration more broadly.

Introduction

Structural colours are some of the most vivid and striking colours found in nature. They are formed from the reflection and refraction of light from physical ultrastructures and examples of these can be found in nearly all groups of organisms. The structural colours of butterflies and moths are among the best described and play diverse roles, including initiation of courtship and mating behaviour [1,2], sex and species discrimination [1,3], long distance mate recognition [4] and signalling of quality and adult condition [5].

Butterflies and moths have evolved several mechanisms of structural colour production by modifying different components of scale morphology [6,7]. Scales typically consist of a flat lower lamina connected to an upper lamina by pillar-like trabeculae, with a small space separating the upper and lower laminae. The lower lamina can act as a thin film reflector that produces hues ranging from violet to green depending on its thickness [8–10]. The upper lamina has a more complex structure; it consists of a parallel array of ridges connected by cross-ribs, and modifications to these can yield diverse optical effects. For example, a lamellar structure in the ridges forms multilayer reflectors that produce the iridescent blue in *Morpho* butterflies [11] and the UV reflectance found in *Colias eurytheme* [12,13]. The variations in hue and brightness of colour produced in the intricate structures of the upper lamina depend on an interplay between the number of lamellae, the thickness of each layer and the spacing between the ridges [14]. It has also been shown that butterflies can tune the structures of the upper lamina to achieve the opposite effect, resulting in a substantial reduction of light reflection. Species with ultra-black wings use a combination of thicker trabeculae, reduced cross-rib spacing, and ridges with a steep shape to funnel the light into melanin granules, thus strongly increasing its absorption [15,16].

Recent studies have begun to uncover the genetic and developmental basis of structural colours in some species [7], revealing a common pattern in *Bicyclus anynana* and *Junonia coenia*; artificial selection for colourful phenotypes quickly resulted in changes in lower lamina thickness, and consequently hue, in a relatively small number of generations [8,10]. On the other hand, knockouts of known colour pattern genes [17], and genes involved in pigment synthesis pathways [18,19], have

shown that modification of these can result in altered scale ultrastructure, and moreover has brought out unexpected instances of structural colour [18]. Interestingly, there are groups of butterflies for which the gene *optix,* a known major colour pattern gene [20], can jointly control pigment based colouration and thickness of the lower lamina, producing blue structural colour [10]. It remains unclear whether this joint control extends to other butterfly taxa that produce structural colour using lower lamina reflection. In species with ridge reflectors, such as *Heliconius,* this does not seem to be the case [18]. More efforts are required to understand the genetic underpinnings and evolution of upper lamina architecture and the organisation of reflective nanostructures in the scales of iridescent butterflies.

Wing colour patterns have been widely studied in the *Heliconius* butterflies, a group of butterflies with a diverse set of aposematic colour patterns. These patterns show examples of both convergent evolution between distantly related species, and divergent evolution within species. Some species form mimicry rings, in which wing patterning is under strong positive frequency-dependent selection due to predation [21]. Pigment colour patterns are largely determined by a small number of genes which are homologous across species. Extensive research has uncovered a toolkit of five loci which control much of the colour pattern variation in *Heliconius* species, and some other Lepidoptera [22]. *Heliconius* also display structural colour, and in comparison to the well-studied pigment colours, very little is known about the development and genetic basis of these. From previous work, we know that certain aspects of scale morphology affect the production of iridescent colouration, a type of angle-dependent structural colour [14,23]. While overall scale morphology is similar between iridescent and non-iridescent scales, those with blue structural colour have overlapping ridge lamellae which act as multilayer reflectors (as in *Morpho*), along with a greater density of ridges on the scale (narrower ridge spacing).

Structural colour has evolved multiple times within the *Heliconius* genus [14]. In some species, all subspecies have iridescent colour, while others exhibit interspecific variation in iridescence. *Heliconius erato* and *Heliconius melpomene* are two co-mimicking species which diverged around 10-13 Mya [24] with each evolving around 25 different colour pattern morphs [25]. Most of the

92 different colour patterns are produced by pigment colours, but subspecies found west of the Andes in
93 Ecuador and Colombia also have an iridescent blue structural colour. *H. erato cyrbia* and *H.*
94 *melpomene cythera* found in Western Ecuador have the brightest iridescence, while subspecies *H.*
95 *erato demophoon* and *H. melpomene rosina,* found to the north in Panama, are matt black in the
96 homologous wing regions (Figure 1). A hybrid zone forms between the iridescent and non-iridescent
97 groups where they meet near the border between Panama and Colombia, and here, populations with
98 intermediate levels of iridescence can be found [26]. Continuous variation in iridescent colour is
99 observed in the centre of the hybrid zone and in experimental crosses [23], suggesting that this trait is
100 controlled by multiple genes. The evolution of pigmentation and simple colour pattern traits have
101 frequently been shown to involve the re-use of a small number of genes across animal species
102 [22,27,28]. However, we may expect the genetic basis of a quantitative trait controlled by multiple
103 genes, such as iridescence in these species, to be less predictable [29]. In addition, iridescence in *H. e.*
104 *cybria* is much brighter than in *H. m. cythera* [14], suggesting some differences in scale structure and
105 presumably genetic control of this structure formation process.

106 Here we use crosses between subspecies of iridescent and non-iridescent *Heliconius* to determine the
107 genetics of both colour and scale ultrastructure traits for the first time. We measure the intensity of
108 blue colour and overall luminance (brightness) to assess variation in colour. We complement our
109 estimates of colour variation with high throughput measurements of ridge spacing and cross-rib
110 spacing using ultra small-angle X-ray scattering (USAXS). Using a quantitative trait locus (QTL)
111 mapping approach, we can identify the location and effect sizes of loci in the genome that are
112 controlling variation in iridescent colour. Comparison of the genetic basis of these traits between *H.*
113 *melpomene* and *H. erato*, two distantly related mimetic species, allows us to ask whether, like pigment
114 colour patterns, variation in iridescent colour and scale structure is also an example of gene reuse.

Results

Experimental crosses

Experimental crosses were performed using geographical morphs of both *Heliconius erato* and *Heliconius melpomene*. In both species, morphs from Panama (*H. e. demophoon* and *H. m. rosina*) were crossed with morphs from Western Ecuador (*H. e. cyrbia* and *H. m. cythera*), then the F1 generation crossed with each other to produce an F2. For *H. erato*, we also analysed a backcross between the F1 and *H. e. cyrbia* (Figure 1). Due to a mix-up in the insectary, one of our largest *H. melpomene* broods, named 'EC70', was obtained from a cross between an F1 father and a mother of unknown parentage, likely an F2 individual. Further details of the crosses are in Table S1.

In the offspring of these crosses, we measured four phenotypes - blue colour (BR), luminance, ridge spacing and cross-rib spacing. 'BR' is the average blue pixel value relative to red, extracted from RGB values from photographs. This was used as a measure of blue hue, while luminance measured overall brightness. Scale structure measurements were extracted from small angle X-ray scattering data from a single family of each species.

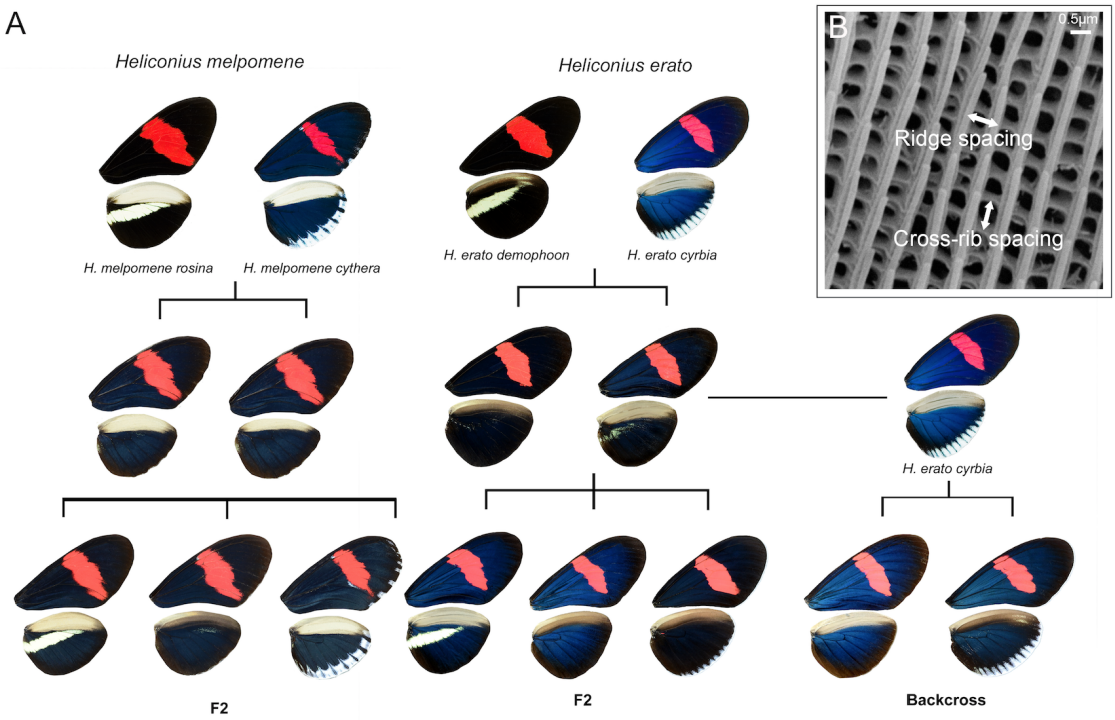

Figure 1. (A) Crosses between iridescent and non-iridescent morphs of *Heliconius melpomene* and *Heliconius erato*. For *H. melpomene* we used F2 crosses, plus one cross thought to be F1xF2 (not shown). For *H. erato*, we used F2 crosses and a backcross to the iridescent race. (B) Electron microscope image of a *Heliconius erato cyrbia* wing scale showing the analysed scale structure measurements.

Phenotypic variation

Based on current understanding of the reflective structures in *Heliconius* and other butterflies [14,30], we predict that reduced ridge spacing should increase the brightness of the reflectance from the wing due to the increased density of reflective structures (ridges) on the wing. However, there are other aspects of scale nanostructure that we would also expect to affect colour hue and brightness, particularly lamellae layering. These aspects could correlate with ridge spacing if they are controlled by the same genetic and developmental mechanism, or they could be controlled independently. The extent to which the different aspects of colour and scale structure are correlated in our broods gives an initial approximation of the extent of genetic correlation between these traits, and therefore the extent to which we are likely to find that they are controlled by the same or different genetic loci. For the *H. erato* family for which we have USAXS measurements, we found significant correlations between scale structure and colour measurements: ridge spacing has a negative correlation of moderate

strength with both BR value (Spearman's rho = -0.411, n = 56, p = 0.0013) and luminance (Spearman's rho = -0.46, n = 56, p = 0.0002, Figure 2), as expected. We also found significant correlations between ridge and cross-rib spacing (Spearman's rho = 0.342, n = 56, p = 0.008) and between BR value and luminance (Spearman's rho = 0.341, n = 56, p = 0.008). Cross-rib spacing is negatively correlated with BR value (Spearman's rho = -0.325, n = 56, p = 0.012) but not with luminance (Spearman's rho = -0.18, n = 56, p = 0.17).

On the other hand, the *H. melpomene* family only showed significant correlations for BR value and luminance (Spearman's rho = 0.295, n =73, p = 0.008) but no correlations were found for BR value and ridge spacing (Spearman's rho = 0.0012, n = 73, p = 0.991), luminance and ridge spacing (Spearman's rho = -0.117, n = 73, p =0.306, Figure 2), ridge spacing and cross-rib spacing (Spearman's rho = -0.088, n = 73, p = 0.441), BR value and cross-rib spacing (Spearman's rho = 0.05, n = 73, p = 0.622) or luminance and cross-rib spacing (Spearman's rho = 0.13, n = 73, p = 0.226). This separation of ridge spacing and colour variation may have arisen in *H. melpomene* as a result of a higher number of generations of mixing in the brood we used (EC70) in comparison to the *H. erato* brood. However, it would also be consistent with a greater genetic correlation between multiple aspects of scale structure in *H. erato* than in *H. melpomene*.

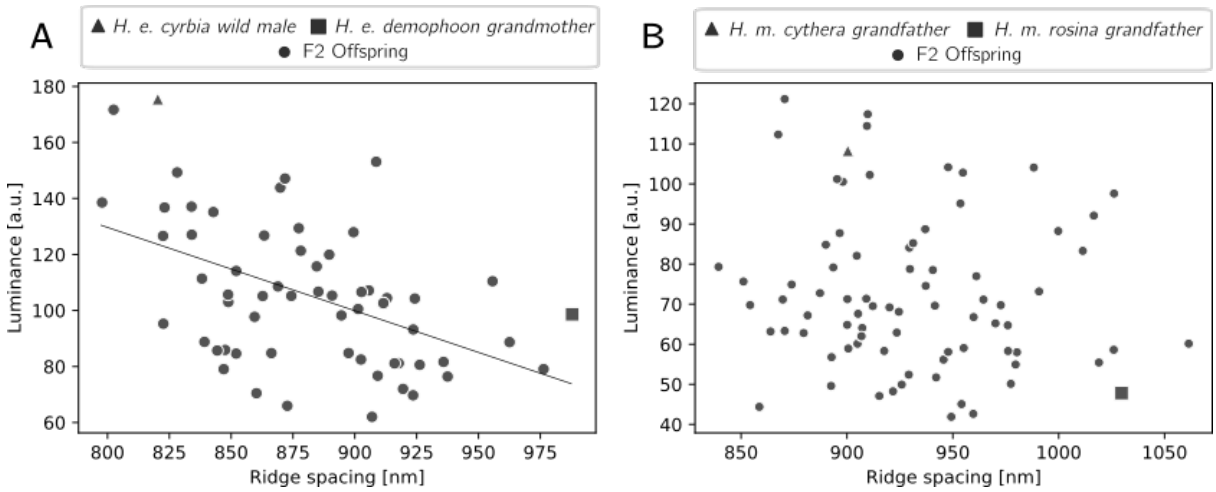

Figure 2. Relationship between ridge spacing and luminance in F2 offspring of *H. erato* (A) and *H. melpomene* (B). A significant correlation was found for *H. erato* only.

170 We tested for sexual dimorphism in the four traits and did not find any significant differences between
171 male and female *H. melpomene* offspring from the largest brood (EC70) in all four traits (Table S2).
172 Sexual dimorphism in *H. erato* was analysed in our previous study, finding differences in all four
173 phenotypes in offspring with a maternal *cyrbia* grandfather [23]. Our sample size from the parental
174 subspecies is small but did not reveal any large difference between the sexes for any of the traits
175 measured, suggesting that the difference we see between the sexes in the crosses are largely due to
176 sex-linkage, as we previously proposed [23]. Nevertheless, we included sex as a covariate in all our
177 subsequent analyses to control for the possibility of slight sexual dimorphism.

178 *QTL mapping in H. erato*

179 Significant QTL were found for three phenotypes in *H. erato* - BR colour, luminance and ridge
180 spacing (Figure 3, Table 1, Table S3). When analysing the colour measurements, F2 and backcross
181 genome scans were combined, and for BR values showed 2 significant QTL on chromosomes 20 and
182 the Z sex chromosome. These were also found when analysing the F2 broods separately from the
183 backcross brood (Figure S1). The intervals around these QTL each contain around 150 genes. At both
184 markers, individuals with Panama-type genotypes (Pan/Pan and Pan(W)) had lower BR values than
185 Ecuador-type and heterozygous genotypes, following the expected trend (Figure 4). Only two
186 individuals have homozygous Panama-type *demophoon* genotypes at the Z chromosome marker due
187 to the small number of individuals with a *demophoon* maternal grandfather (Table S1). The QTL on
188 the Z chromosome explained the largest proportion of the phenotypic variation in BR colour in both
189 the F2 crosses (19.5%) and the backcross (24.6%), and the chromosome 20 QTL explained a further
190 12.3%.

191 Luminance (overall brightness of the wing colour) was highly associated with the Z chromosome
192 (Figure 3B). The significant marker did not map exactly to the same position as for the BR values but
193 was apart by only 3.6cM, and confidence intervals for each overlap. Individuals with Ecuador-type
194 alleles had higher luminance values than those with Panama-type alleles, showing the same trend as
195 the BR values (Figure 4). This QTL explained 40.2% of the variance in luminance values in the F2

196 crosses and 24.2% in the backcross. This was the only significant QTL for luminance, with nothing
197 appearing on chromosome 20.

198 A single QTL on the Z chromosome was also significant for ridge spacing (Figure 3C). This marker
199 was at a different position to the markers for BR and luminance, which may be due to using only one
200 family for this analysis, although the confidence intervals overlap. When we repeated the analysis for
201 luminance using only this family, the same marker showed the highest LOD score for both luminance
202 and ridge spacing (Figure S1). All genotypes with one or two Ecuador-type alleles had similar ridge
203 spacing, but those with a hemizygous Panama-type genotype ('Pan(W)' in Figure 4) had significantly
204 wider ridge spacing. This QTL explained 34.8% of variance in ridge spacing in this family. No
205 significant QTL were found for cross-rib spacing, although the highest LOD score was seen on the Z
206 chromosome (Figure 3D).

207

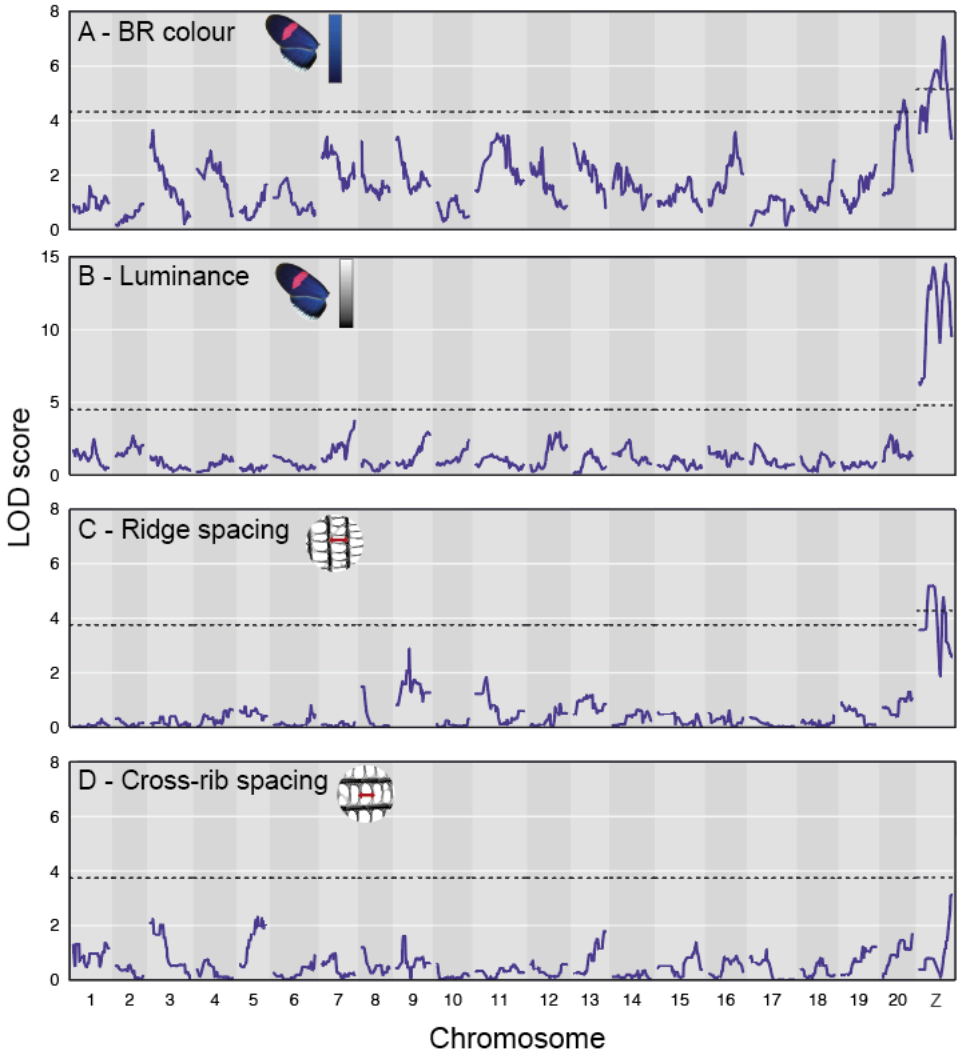

Figure 3. *H. erato* QTL plots including all families for BR colour (A) and luminance (B). QTL plots for a single family for ridge spacing (C) and cross-rib spacing (D). Dotted line shows p=0.05 significance level.

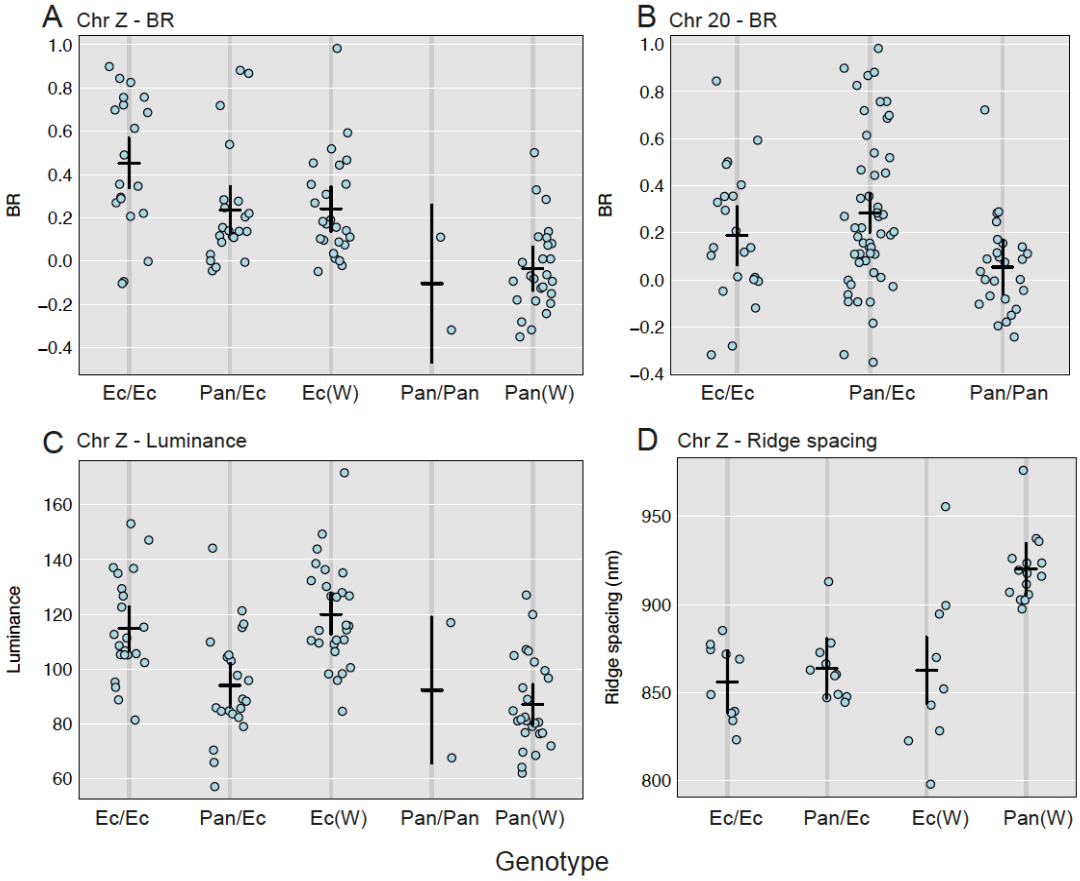

Figure 4. The phenotypes of F2 individuals with different genotypes at the most significant markers within each *H. erato* QTL. The QTL for BR on the Z chromosome (A) and chromosome 20 (B). Significant Z markers for luminance (C)and ridge spacing (D). 'Pan' denotes alleles from the Panama race *demophoon*, and 'Ec' the Ecuador race *cyrbia*. Marker positions are shown in Table 1.

Phenotype	Marker	Chromosome	Position (cM)	LOD	p
Heliconius erato					
BR colour (all families)	Herato2101_12449252	Z	38.0	7.07	0.001
	Herato2001_12633065	20	32.9	4.75	0.022
Luminance (all families)	Herato2101_12449398	Z	41.6	14.50	<0.001
Ridge Spacing (single family)	Herato2101_7491127	Z	23.0	5.21	0.013
Heliconius melpomene					
BR (all families)	Hmel203003o_2119654	3	15.22	7.26	0.001
Luminance (all families)	Hmel203003o_2635435	3	17.97	13.61	<0.001
Ridge spacing (EC70)	Hmel207001o_11550301	7	53.61	5.71	<0.001

Table 1: Significant QTL found for three phenotypes in *H. erato* and *H. melpomene*.

220 *QTL mapping in H. melpomene*

221 Genome scans for three F2 families were combined with scans of the EC70 brood. Since the
222 parentage of the mother of the EC70 brood is unknown, the maternal alleles in the offspring could not
223 be assigned as being from either a *cythera* or a *rosina* grandparent. Therefore, in this family only
224 paternal alleles were taken into account (and all maternal alleles set to 'A'), and the cross was treated
225 as if a backcross. A single significant QTL for BR colour was found on chromosome 3 (Figure 5A,
226 Table 1, Table S4). The interval around this marker relates to a genomic region of approximately
227 3Mbp and contains 130 genes. The marker explains 15.3% of phenotypic variation in EC70 (which
228 will be an underestimate due to all maternal alleles being assigned to the same genotype) and 9.2% in
229 the three F2 families. This suggests that there will be other loci in the genome with effects on colour
230 that we lack the power to detect. A marker on chromosome 10 shows a high LOD score that does not
231 reach significance, but could be suggestive of a locus on this chromosome. This is clearer when
232 looking only at the three F2 families separated from the EC70 brood (Figure S2). This marker
233 explains 17% of variation in the F2 families. Chromosome 10 contains the *WntA* gene, which controls
234 pigment colour pattern elements, however the QTL interval does not overlap with this. Luminance
235 was also strongly associated with markers on chromosome 3 (Figure 5B). The significant marker was
236 2.75cM from the marker for BR colour, and the confidence intervals overlap. In contrast, for ridge
237 spacing we found a significant QTL on chromosome 7 (using just the EC70 brood), explaining 30.3%
238 of variation (Figure 5C). Again, no significant QTL were found for cross-rib spacing (Figure 5D).

239 Individuals with homozygous Panama-type genotypes at the mapped chromosome 3 markers had
240 lower BR and luminance values (Figure 6). Individuals carrying Ecuador-type alleles at the mapped
241 chromosome 7 marker showed reduced ridge spacing, consistent with the observation that the Panama
242 race has greater ridge spacing and that this is associated with a lack of iridescence.

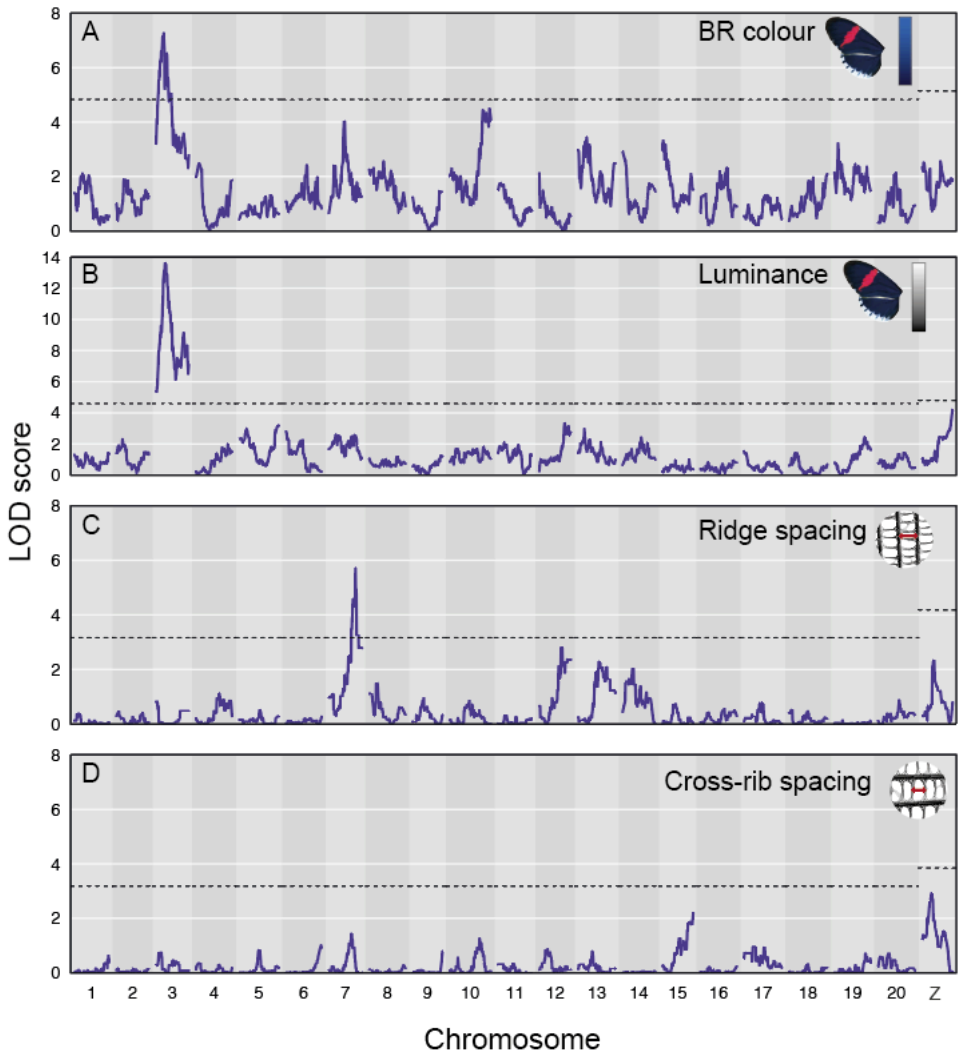

Figure 5. *H. melpomene* QTL plots including all families for BR colour (A) and luminance (B). QTL plots for a single family for ridge spacing (C) and cross-rib spacing (D).

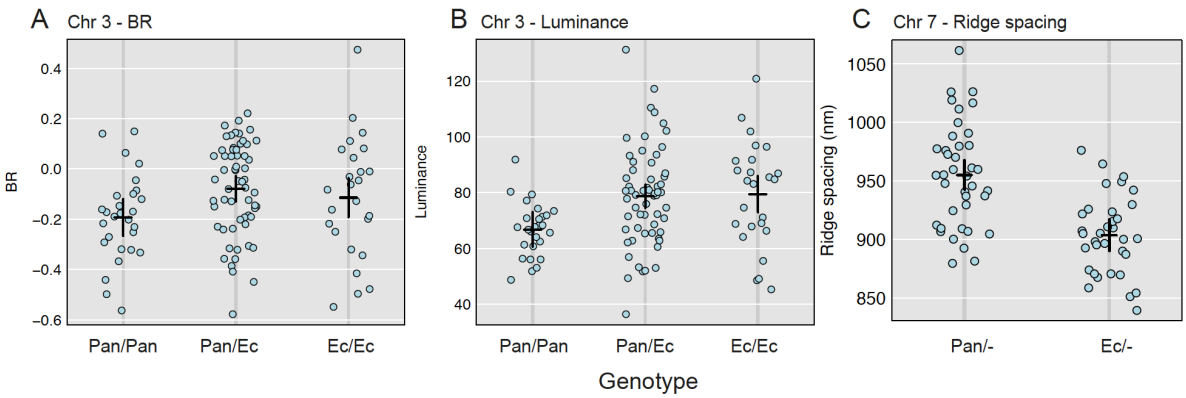

Figure 6. Genotype x phenotype plots for significant *H. melpomene* QTL. For the F2 families: (A) BR colour and (B) luminance. 'Pan' denotes alleles from the Panama race *rosina*, and 'Ec' the Ecuador race *cythera*. (C) Ridge spacing in the EC70 brood. Here we only know the origin of the paternal allele. Marker positions shown in Table 1.

252 *Association analysis for H. melpomene*

253 Treating the EC70 cross as a backcross is not ideal as it ignores potentially interesting genetic
254 variation that is segregating from the mother (which phenotypically and genetically appeared to be an
255 F2 individual), and could lead to artefacts. Therefore, we also conducted a SNP association analysis
256 including the full set of *H. melpomene* broods (F2 + EC70) and for the EC70 family alone, using a
257 family-based score test for association [31] and controlling for family structure [32].

258 The GWAS of the EC70 family did not reveal significant genetic associations for either of the scale
259 structure traits (Figure S3). The SNPs with the lowest p-values were found on chromosomes 1, 7, 17
260 and Z for ridge spacing, and on chromosomes 13 and Z for cross-rib spacing. Similarly, we did not
261 find significant associations between SNPs and BR values in EC70, although the lowest p-values were
262 found on chromosome 3 and chromosome 10, which aligns with the QTL results. We did find SNPs
263 significantly associated with variation in luminance on chromosome 3, with a single SNP scoring
264 above both conservative genome-wide Bonferroni corrected thresholds. When analysing all of *H.*
265 *melpomene* broods together accounting for pedigree structure, we found significant associations for
266 both colour traits (BR value and luminance) on chromosome 3. Stronger support for association was
267 found for luminance in comparison to BR value. Overall, the association analysis results supported
268 the QTL results but did not reveal additional loci.

269 *Location of pigmentation pathway genes*

270 Previous studies have shown that genes belonging to pigmentation pathways have an effect on both
271 pigmentation and scale structure in butterflies. Matsuoka and Monteiro [19] tested the effect of genes
272 from melanin and ommochrome synthesis pathways and found that 2 out of 8 genes tested had an
273 effect on the modification of scale structure. We queried the position of these 8 genes (*DDC, yellow,*
274 *aaNAT, pale, ebony, vermillion, white* and *scarlet*) in the genomes of *H. erato* and *H. melpomene* to
275 assess whether our QTL overlapped any of these genes (Table S5). In addition, we queried the *tan*
276 gene which is involved in cuticular melanisation [33] and is up-regulated in melanic regions of
277 *Heliconius* butterflies [34]. We found that the pigmentation genes belonging to the ommochrome and

278 melanin pathways have similar physical locations in the genomes of *H. erato* and *H. melpomene*, as
279 expected due to their high level of synteny. None of the pigmentation pathway genes are located
280 within the Bayesian confidence intervals estimated for the QTL found in either species for structural
281 colour or scale structure variation. However, we found that the *tan* and *pale* genes, both belonging to
282 the melanin pathway, are located on the Z sex chromosome. The *pale* gene is located at a physical
283 position that is 1 Mbp and 724 kbp from the upper limits of the Bayesian confidence intervals of the
284 QTL found for ridge spacing and luminance respectively in *H. erato,* and *tan* is located approximately
285 1.76 Mbp and 1.2 Mbp from the lower limits of the confidence intervals of the same QTL.

286

287 **Discussion**
288
289 In one of the first studies to look at the genetics of structural colour variation in terms of both colour
290 and structure, we show that the trait is controlled by multiple genes in the co-mimics *Heliconius erato*
291 and *Heliconius melpomene*. While we found only a small set of significant loci, these explain
292 relatively little of the overall phenotypic variation, suggesting there are more loci which remain
293 undetected. We found evidence for a genetic correlation between two aspects of structural colour
294 variation – BR value for hue and luminance for brightness. Within each species these were controlled
295 by loci on the same chromosomes. In *H. erato*, this was on the Z chromosome, confirming our
296 previous phenotypic analysis [23], and in *H. melpomene*, on chromosome 3. An additional locus on
297 chromosome 20 was also found to affect blue colour but not brightness in *H. erato*. Brightness of
298 iridescent colour is predicted to be controlled primarily by the number of layers within the multilayer
299 reflector structure, while hue is predicted to be controlled by the thickness and spacing of the layers
300 [35]. A genetic correlation between these two aspects of colour would suggest that both aspects of
301 scale nanostructure are controlled by these genetic loci. This would be advantageous in the evolution
302 of structural colour by allowing concerted changes in both aspects required for colour production. In
303 contrast, the presence of a possible independent hue modifier locus on chromosome 20 in *H. erato*
304 would allow more evolutionary flexibility in the colours that could be produced.

305 We also found correlations between colour, brightness and ridge spacing in *H. erato*. The Z
306 chromosome locus appears to control ridge spacing, which could have a direct effect on the brightness
307 of the reflectance by increasing the density of reflective structures. As further proof of this, in the
308 single-family analyses, luminance and ridge spacing mapped to exactly the same marker.
309 Alternatively, the observed correlation between brightness and ridge spacing in *H. erato* may be a
310 product of an unobserved association between tighter ridge spacing and other aspects of scale
311 nanostructure, specifically the number of lamellae layers within the ridges. Theoretical analyses and
312 simulations of the optical properties of multilayers have revealed that increasing the number of layers
313 will result in a rapid increase of brightness; adding even a small number of layers produces a
314 significant increase in the amount of reflected light [36]. Therefore, the Z chromosome locus may be
315 affecting multiple aspects of scale structure, producing the observed correlations between the different
316 colour and structure measurements. Also consistent with this is the evidence for a genetic correlation
317 between ridge and cross-rib spacing in *H. erato.* The effect of the Z locus on cross-rib spacing did not
318 reach significance, but had the highest genome-wide LOD score. Cross-rib spacing is not predicted to
319 have an effect on colour but could have a developmental correlation with ridge spacing.

320 In contrast, these correlations are not seen in *H. melpomene*, with different loci controlling colour and
321 ridge spacing, suggesting a more dispersed genetic architecture and different loci controlling different
322 aspects of scale structure. We found strong evidence for a locus on chromosome 3 controlling BR and
323 luminance, but this locus appeared to have no effect on our measurements of scale structure and so is
324 likely controlling other aspects of scale structure not quantified here. Instead, we find a locus on
325 chromosome 7 that partially controls ridge spacing. We see a small, but not significant, effect of this
326 chromosome on BR colour, suggesting that ridge spacing may have a small and relatively weak effect
327 on colour in *H. melpomene*, despite the parental populations showing a similar difference in ridge
328 spacing to that seen in *H. erato*. Differences in the experimental crosses between species may have
329 influenced these results, with the analysis in *H. melpomene* using only paternal alleles, and so having
330 reduced power. Nevertheless, the Z chromosome QTL has an effect of similar size on ridge spacing
331 and brightness in *H. erato* and no other loci affecting ridge spacing were detected in *H. erato*,

332 suggesting that the detection of different loci controlling colour and ridge spacing in *H. melpomene*
333 cannot be explained by reduced power. If *H. erato* has a locus on the Z chromosome that can control
334 multiple aspects of scale structure, while *H. melpomene* requires mutations at loci dispersed around
335 the genome, this could provide one explanation for how *H. erato* has been able to evolve brighter
336 structural colour than that observed in *H. melpomene*. Measuring and quantifying the lamellar
337 structure in large numbers of individuals is a major technical challenge but could be an important next
338 step in understanding the genetic control of butterfly structural colour.

339 In contrast to many of the loci for pigment colour patterns which are homologous across multiple
340 *Heliconius* species, the loci controlling iridescence in *H. erato* and *H. melpomene* appear to be
341 different. Differences in the physical scale architecture and brightness of colour between the species
342 perhaps makes these genetic differences unsurprising [14,26]. A lack of genetic parallelism may also
343 be more likely for a quantitative trait such as iridescence [29]. Shared standing genetic variation can
344 lead to repeated use of certain genes, as is seen in the repeated adaptation of sticklebacks to freshwater
345 environments [37,38]. The differences in genetic architecture between species suggest this is unlikely
346 to be the case for iridescence in *Heliconius* and that the trait likely evolved due to multiple,
347 independent genetic mutations. Nevertheless, on the Z chromosome in *H. melpomene*, we do observe
348 elevated LOD scores in the QTL analysis and low p-value SNPs in the GWAS for both scale structure
349 traits, but neither of the colour traits. This suggests that *H. melpomene* may have a locus homologous
350 to that in *H. erato,* which is controlling some aspects of scale structure variation, but with apparently
351 little or no effect on colour variation.

352 One limitation of our approach is that the accuracy of QTL analyses is limited, particularly when
353 sample sizes are relatively small, as they are here, resulting in inflated estimates of explained variance
354 [39]; the percentages of explained variance we report are probably an overestimate due to the Beavis
355 effect [40]. Therefore, the QTL we detected likely explain the most variation in these particular
356 families, and other QTL that remain undetected possibly could be shared between species. Thus, we
357 cannot discard a scenario of a partially shared genetic architecture for scale structure and luminance.

358 Differences in the ecology and selective forces shaping colour traits between species could also
359 explain differences in the genetic basis of structural colour. Comparisons of the hybrid zones in both
360 species have revealed much broader clines in iridescent colour in *H. melpomene* compared to *H.*
361 *erato*, suggesting that it is under weaker selection in *H. melpomene* [26]. In addition, loci controlling
362 sexually selected traits are expected to accumulate on the sex chromosomes [41,42]. Sex-linkage of
363 this trait in *H. erato* could therefore be consistent with iridescent colour being sexually selected in this
364 species. Unpublished reflectance data also support greater sexual dimorphism in iridescent colour in
365 *H. erato* than in *H. melpomene* [43]. Disentangling cause and effect in this case is clearly complex
366 and experimental studies are needed to determine what function iridescence plays in these species.

367 In recent years, reverse genetics research has revealed a surprising connection between the molecular
368 machinery underlying the development of pigmented wing patterns and the ultrastructure of butterfly
369 scales in various species [17–19,44,45]. In particular, knock-outs of two of the major colour pattern
370 controlling loci, *optix* and *WntA,* have been shown to affect aspects of scale structure [10,17,18,44].
371 However, our QTL are not associated with any known colour pattern gene of large or small effect.
372 The known toolkit of colour-pattern controlling loci are located on chromosomes 1, 10, 13, 15 and 18
373 (*aristaless, WntA, vvl*, *cortex* and *optix* respectively) in *Heliconius* [22] while the QTL we detect are
374 on chromosomes 3, 7, 20 and 21 (the Z chromosome). Hence, our findings show that *H. erato* and *H.*
375 *melpomene* do not use the known molecular machinery of wing pattern production for sculpting
376 specialised nanostructures and iridescent wings.

377 Genes involved in pigment production pathways in insects have also been found to have an effect on
378 the architecture of the butterfly scale. Knockouts for two genes of the melanin-dopamine pathway
379 produced modifications of the scale architecture [19,46]. Our examination of the locations of melanin
380 and ommochrome production genes did not reveal an overlap with the QTL or their estimated
381 confidence intervals in any of our crosses. We found QTL on the same linkage group as two melanin
382 pathway genes, but despite this, the evidence suggests that these genes are not involved in scale
383 structure modification in *Heliconius,* as they fall outside the confidence intervals of the QTL. The
384 evidence we present here, together with previous reverse genetics research on *Heliconius* [17,18]

385 suggest that the genetic architecture of iridescent structural colour produced by ridge reflection in *H.*
386 *erato* and *H. melpomene* is completely decoupled from that of mimicry related wing pattern regulation
387 and that of pigment production. Furthermore, the QTL that we found here do not overlap with QTL
388 for pigment pattern variation that were found in a super-set of the families that we have used here
389 [47], further supporting the idea that structural colour variation and wing pattern variation is unlinked
390 in both species.

391 Overall, we show that evolution has targeted different sets of genes to develop scale architecture
392 suitable for structural colour production in *H. erato* and *H. melpomene*. The lack of gene reuse in the
393 evolution of this complex quantitative trait may be due to a joint effect of the ecological role of
394 structural colour shaping the mutational landscape differently in both species, and also of a presumed
395 less constrained evolutionary pathway due to the increased availability of loci of small effect that can
396 potentially evolve iridescent blue phenotypes. Although our forward genetics approach does not
397 single out specific genes, it has revealed novel loci of morphological evolution in butterflies. Gene
398 expression and functional studies could follow up genes in these QTL intervals to understand the role
399 these play in sculpting colour-producing nanostructures.

400 **Methods**

401 *Sampling*

402 Non-iridescent *H. erato demophoon* and *H. melpomene rosina* were collected from Gamboa, Panama
403 (9.12ºN, 79.67ºW). Iridescent *H. erato cyrbia* and *H. melpomene cythera* were collected from the area
404 around Mashpi, Ecuador (0.17ºN, 78.87ºW). Within a few hours of emergence, wings of offspring
405 were removed and stored in glassine envelopes and bodies were stored in NaCl saturated 20%
406 dimethyl sulfoxide (DMSO) 0.25M EDTA solution to preserve the DNA. A total of 155 *H. erato*
407 individuals from 5 broods were used to generate linkage maps and perform QTL mapping (3
408 *demophoon* and 3 *cyrbia* grandparents, 11 F1 parents, and 40 backcross and 99 F2 offspring). For *H.*
409 *melpomene*, data from 4 broods made up of 228 individuals were used (1 *rosina* and 2 *cythera*
410 grandparents, 5 F1 and 219 offspring, and 1 unknown parent). Many samples analysed in this study
411 were previously used in Brien et al. [23] and Bainbridge et al. [47]. Further details of crosses and
412 samples used in each analysis can be found in Table S1.

413 *DNA extraction and sequencing*

414 Genomic DNA was extracted from approximately half of the thorax of each individual using the
415 Qiagen DNeasy Blood & Tissue kit. Single-digest Restriction site-associated DNA (RAD) library
416 preparation and sequencing were carried out by the Edinburgh Genomics facility. DNA was digested
417 with the enzyme *PstI*, and libraries were sequenced on an Illumina HiSeq 2500 producing 125bp
418 paired-end reads. Parents of the crosses (16 *H. erato* and 9 *H. melpomene*) were included at 2x higher
419 concentration within the pooled library to produce a higher depth of coverage.

420 *Data processing and linkage map construction*

421 Sequence data processing and linkage map construction are described in detail in Bainbridge et al.
422 [47]. Briefly, RAD sequences were demultiplexed using the RADpools function in RADtools (v1.2.4,
423 [48]). FASTQ files were mapped to the *H. erato* v1 reference genome [49] or the *H. melpomene* v2.5
424 reference genome [50] using bowtie2 v2.3.2 [51]. BAM files were then sorted and indexed with

425 SAMtools (v1.3.1, [52]) and PCR duplicates were removed using Picard tools MarkDuplicates
426 (v1.102). SAMtools mpileup and Lep-MAP data processing scripts [53] were used to call genotype
427 posteriors.

428 Linkage maps were constructed with Lep-MAP3 [53], using the modules ParentCall2 (with options
429 ZLimit=2 and removeNonInformative=1), Filtering2, SeparateChromsomes2 (using sizeLimit = 50
430 and a LOD score of 12 for *H. erato* and 23 for *H. melpomene*) and JoinSingles2All. Finally, the
431 module OrderMarkers2 was used to order the markers along the linkage groups, taking into account
432 the genomic positions of the markers. Female recombination was set to 0 and male recombination set
433 to 0.05 (following [54]). We used LMPlot to visualise the maps and check for errors in marker order.
434 Any erroneous markers that caused long gaps at the beginning or ends of the linkage groups were
435 manually removed. Genotypes were phased using Lep-MAP's map2genotypes.awk script, and
436 markers were named using the map.awk script and a list of the SNPs used to provide the scaffold
437 name and position. The final linkage maps contained 5648 markers for *H. erato*, and 2163 markers for
438 *H. melpomene*.

439 *Measurements of colour variation*

440 Wings were photographed under standard lighting conditions (full details in [23]). A colour checker in
441 each photograph was used to standardise the photographs using the levels tool in Adobe Photoshop
442 (CS3). RGB values were extracted from two areas of each wing (proximal areas of both the forewing
443 and hindwing) and averaged. Blue-red (BR) values were used as a measure of blue iridescent colour.
444 These were calculated as (B-R)/(B+R), where +1 is completely blue and -1 is completely red.
445 Luminance measured overall brightness and was calculated as R+G+B, with each colour having a
446 maximum value of 255.

447 *Measurements of scale structure variation using ultra small-angle X-ray scattering (USAXS)*

448 The USAXS experiment was carried out at the ID02 beamline at the European Synchrotron (ESRF,
449 Grenoble, France). We examined scale structure variation for one family of each species (n=56 *H.*
450 *erato* F2 and n=73 *H. melpomene* (unknown mother)). We measured between 33 and 113 points per

individual along a linear proximodistal path across the proximal part of the forewing, which has the most vivid iridescence in the blue subspecies (Figure S4). The X-ray beam wavelength was $\lambda = 1$Å and it had 12.45 keV energy. The beam was collimated to a section of 50 µm × 50 µm to probe a small area within a single scale. The scattered radiation was recorded with a high-sensitivity FReLon 16M Kodak CCD detector with an effective area of 2048 × 2048 pixels and a 24 µm pixel size, a sample to detector distance of 30.7m, accessible q range between 8.5x10-4 nm^{-1} and 3.8x10-2 nm^{-1}, and limited interpretation of structure spacing to above 160 nm. The raw images were corrected for dark current and spatial distortion.

Scanning electron microscopy (SEM)

SEM on a small subset of individuals was used to confirm our scale structure measures from the USAXS data. We sampled four iridescent *H. e. cyrbia* and three *H. m. cythera*, and eight *H. e. demophoon* and three *H. m. rosina* with black pigment colour. Representative SEM images of dorsal cover scales for each of the four races used are in Figure S5. First, we compared ridge spacing of blue individuals vs. black individuals on the dorsal side. This allowed us to gauge the expected range of scale structure variation in blue and black coloured scales. Secondly, we compared ridge spacing of dorsal vs. ventral scales within each race. This comparison allowed us to separate signals coming from overlapping scales in the USAXS experiment.

Wing samples were cut from the region of interest shown in Figure S4. We mounted samples on aluminium SEM stubs using 9mm adhesive carbon tabs and coated them with a thin layer of gold using vacuum evaporation. Samples were imaged on a JEOL JSM-6010LA microscope and we used the InTouchScope software to take images of the regions of interest at a magnification level of 900X. Images included both cover and ground scales.

At the midpoint of the scale length, we drew a linear transect perpendicular to the orientation of the ridges (Figure S6). Ridge spacing was calculated using the PeakFinder tool [55]; a plugin for the Fiji [56] image analysis package, using a tolerance level of 60 and a minimum distance threshold of 10 pixels between peaks. PeakFinder detects spikes of intensity along the linear transect, each peak

corresponding to a single ridge. It then yields the distances, in pixels, between subsequent peaks (Figure S6). Using the scale bar of SEM slides we determined the variable rate of conversion from pixels to nm to be 25 x 10^{-3} / M where M is the level of magnification and we used this variable rate to convert distances between ridges to nm and average all distances between ridges to obtain average ridge spacing per scale.

Analysis of USAXS data to extract ridge spacing values

We first did a qualitative joint assessment of our USAXS and SEM data to get an idea of the scale structures we captured in our experiment and how to best get their information. Our interpretation of scale structures in a USAXS scattering pattern is shown in Figure S7. Two important observations come from this joint assessment. Firstly, it can be observed that blobs of scattered radiation distribute along linear paths from the centre of the picture with equal spacing between them (Figure S7 A). This periodic scattering can be understood as the signature of the interaction of the beam with the array of parallel ridges on the surface of the scale (Figure S7 B) [57]. Secondly, the beam goes through the dorsal and ventral sides of the wing, projecting onto the detector, with the scattering due to structures of as many as four scales: cover and ground scales on both dorsal and ventral sides of the wing, in the case that all of them overlap. This can be observed in Figure S7 A, where at least three overlapping scales were picked up by the beam. Our SEM analysis revealed that scales with smaller ridge spacing are found on the dorsal side compared to the ventral side of the wing regardless of the structural colour of the butterfly analysed (Figure S8). These differences in ridge spacing between dorsal and ventral scales should be discernible in the USAXS data.

We used these two observations to implement a script that extracts relevant scale structure information from the USAXS data. The script scans the 2D scattering pattern in non-overlapping regions of 5°. If the region contains periodic scattering it is assumed to correspond to the ridges of the scale and is kept for comparison with other sections that also show periodic scattering. The script keeps the section with the highest magnitude of the scattering vector q based on the observation that q should be larger for dorsal scales because they have tighter ridge spacing. The chosen region is

503 recorded and the scanning section is rotated 85° anti-clockwise to capture the scattering due to cross-
504 ribs, which are perpendicular to ridges in the scale. Azimuthal integration is then performed on the
505 two regions of interest, reducing them to a one-dimensional representation of scattered intensity I as a
506 function of the magnitude of the vector q in a similar way to previous studies [14,23], applying
507 corrections for transmitted flux and masking the pixels corresponding to the beam stop. The script
508 uses the pyFAI [58] and fabio [59] libraries to do the azimuthal integration and USAXS data
509 handling.

510 Despite dividing the scattering pattern in small regions to pick apart the signals due to different
511 structures and scales, some frames still contained information of more than one scale. This happens in
512 the case that overlapping scales have highly similar orientations (i.e. their ridges are parallel or nearly
513 parallel). Thus, a visual inspection was done and we filtered out 1D scattering patterns that contained
514 signals from more than one scale. We also aimed to reduce noise in the scattering signals to improve
515 estimation of dimensions of scale structures. We ran a PCA on the 1D scattering data and retained
516 PCs that cumulatively explained 90% or more of the variation in the data. The original data were
517 projected back onto the retained PCs. The choice of threshold for the percentage variance explained is
518 arbitrary, but we found 90% to be a sensible balance to retain signal but reduce noise.

519 The retained 1D scattering patterns were fit to a Lorentzian curve (Figure S9) using the FitManager
520 module of the silx package [60]. The "center" parameter of the fitting procedure gives the magnitude
521 of the scattering vector q. This magnitude contains information on the distance between peaks of
522 intensity in reciprocal space. To get estimates of structure sizes in real space, we use the expression d
523 $= 2\pi/q$ where d is the distance between ridges or cross-ribs in real space. We averaged estimates of
524 each structure on a per-individual basis to get estimates of average ridge spacing and average cross-rib
525 spacing per butterfly.

526 *Quantitative Trait Locus mapping*

527 The R package R/qtl was used for the QTL analysis [61]. For *H. erato*, initially the F2 crosses were
528 analysed together and the backcross analysed separately. Genotype probabilities were calculated for

529 these two groups using *calc.genoprob*. We ran standard interval mapping to estimate LOD (logarithm
530 of the odds) scores using the *scanone* function with the Haley-Knott regression method. In the F2
531 analysis, sex and family were included as additive covariates, and family was included as an
532 interactive covariate, to allow multiple families to be analysed together. Sex was included as a
533 covariate in the backcross analysis to account for any sexual dimorphism. To determine the
534 significance level for the QTL, we ran 1000 permutations, with *perm.Xsp=T* to get a separate
535 threshold for the Z chromosome. A single F2 family (n=56) was used to analyse scale structure
536 variation (ridge spacing and cross-rib spacing) using the same method, albeit a higher number of
537 permutations was used for determining the significance level of the QTL (4000). For analyses of BR
538 colour and luminance, LOD scores for the F2 crosses and the backcross were added together, to allow
539 analysis of all individuals together to increase power, and the significance level recalculated in R/qtl.

540 Confidence intervals for the positions of QTL were determined with the *bayesint* function and we
541 used a *fitqtl* model to calculate the phenotypic variance that each QTL explained. Genome scan plots
542 and genotype plots were made with R/qtl2 [62]. Genetic distances in the QTL results are based on the
543 observed recombination rate and expressed in centimorgans (cM), which is the distance between two
544 markers that recombine once per generation. These were related to physical distances based on the
545 marker positions in the assembled reference genome of each species.

546 The same method was used to run genome scans for BR colour and luminance in *H. melpomene*. LOD
547 scores of the three F2 families were added to the LOD score from the EC70 family, as in *H. erato*, and
548 the significance level recalculated. Again, a single family was used for analysis of scale structures
549 (n=73).

550 *Association analysis for H. melpomene*

551 The test was done in two steps: in the first step a mixed model is used to get estimates of trait values
552 after adjusting for covariates and random polygenic effects using the linear model:

553 $Y_i = \mu + \sum_j \quad \beta_j C_{ji} + G_i + e_i \quad (1)$

554 In this model we used a genomic kinship matrix to account for pedigree structure. In the model Y_i is a
555 vector of phenotypes for each individual, μ is the mean phenotype for the population, C_{ji} is the value
556 of covariate j for individual i, β_j is the estimated effect for each covariate, G_i are random additive
557 polygenic effects and e_i are the residual effects for each individual. The result of this first part are the
558 trait residuals after accounting for covariates and random polygenic effects and is denoted by $\widehat{e_i}$. The
559 estimates of trait variation that were not explained by kinship or covariates in the first step are then fit
560 to a second model:

561 $$\widehat{e_i} = \mu + \beta g + e_i \quad (2)$$

562 In the second step, β is the parameter for the effect of each SNP tested, g is a single SNP and e_i is the
563 residual variation in phenotype for each individual i. We did the association tests on two sets: the first
564 set included all *H. melpomene* families and two phenotypes; BR value and luminance. The second set
565 included the EC70 family only and four phenotypes: BR value, luminance, ridge spacing and cross-rib
566 spacing.

567 Genotypes were called using the 'mpileup' command in samtools v1.8 [52] with minimum mapping
568 quality set to 20, and the 'call' command in bcftools v1.8 [52] run in consensus mode, with SNP p-
569 value threshold set to 0.05 and calling only variant sites. For our association analyses we kept biallelic
570 SNPs only. We applied the following quality control criteria to our SNP data: we excluded individuals
571 and sites that were not at least 95% genotyped. Sites were also excluded from our analysis if they
572 were not in Hardy-Weinberg equilibrium ($p<0.01$). The MAF threshold was set to the default value
573 (5/2n, where n is the number of individuals). After quality control, we retained 146,122 markers
574 genotyped across 211 individuals for the first set, and 63,132 sites genotyped across 69 individuals for
575 the second set. We set sites called as heterozygous on the sex chromosome in females as missing
576 (females are the heterogametic sex). Multiple testing was accounted for using two thresholds: A
577 Bonferroni corrected threshold calculated as 0.05/k where k is the number of sites analysed, and a less
578 conservative 5% false discovery rate threshold estimated using the GenABEL qvaluebh95 function.

579 *Genes involved in wing pigmentation*

580 We queried the eight pigmentation pathway genes functionally analysed by Matsuoka and Monteiro
581 [19]; five from the melanin-dopamine pathway and three from the ommochrome synthesis pathway,
582 and the *tan* gene, not reported by Matsuoka and Monteiro as having an effect on scale structure, but
583 which is part of the melanin-dopamine pathway in *Heliconius* [34]. We used the common names of
584 these genes to find their start and end coordinates in physical distance using the Ensembl tool
585 available on Lepbase [63]. When the search by name did not produce matches on Lepbase, we queried
586 the common name of the gene on FlyBase (FB2020_05) [33]. We verified manually the matching
587 results using the description of the gene's function. We then obtained its nucleotide sequence and did
588 a BLASTN search [64] against a database comprising all butterfly genomes available on Lepbase. We
589 assumed the top hit on both species to be homologous to the query sequence and used the physical
590 information of these top hits to find the localisation of pigmentation genes in the genomes of *H. erato*
591 and *H. melpomene.*

592 **Acknowledgements**

593 We thank the governments of Ecuador and Panama for permission to collect butterflies. Thanks to
594 Darwin Chalá, Juan López and Gabriela Irazábal for their assistance with the crosses. We are grateful
595 to the European Synchrotron Radiation Facility for provision of X-ray beamtime under proposal
596 LS2720, and to Andrew Dennison for assistance with USAXS data collection. Library preparation and
597 sequencing was performed by staff at the Edinburgh Genomics Facility, at the University of
598 Edinburgh. We thank Vicky Lloyd for assistance with the collection and analysis of SEM data and for
599 helpful comments on the manuscript, and Alan Dunbar for use of the scanning electron microscope.

600 **Data availability**

601 Sequence data have been deposited in the European Nucleotide Archive under project number
602 PRJEB38330. Photographs of all samples can be found at https://doi.org/10.5281/zenodo.3799188.
603 USAXS data handling scripts can be found at https://github.com/juanenciso14/butterfly_usaxs.
604 Linkage maps, QTL scripts and all phenotypic measurements used will be available on publication.

605 **Author contributions**

606 MNB and JER performed the QTL analyses and wrote the manuscript with NJN. PR and MNB
607 constructed the linkage maps. AJP co-ordinated collection of the USAXS data, which were collected
608 by TZ, AJP, EVC, NJN and MNB. JER analysed the USAXS and SEM data and ran the association
609 analysis. PAS, CM, MNB, EVC and NJN performed the crosses. NJN devised and co-ordinated the
610 study. All authors read and commented on the manuscript.

611 **Funding disclosure**

612 This work was funded by the UK Natural Environment Research Council (NERC) through an
613 Independent Research Fellowship (NE/K008498/1) to NJN. MNB and EVC were funded by the
614 NERC doctoral training partnership, ACCE (NE/L002450/1). JER is funded through the Leverhulme
615 Centre for Advanced Biological Modelling as well as scholarships from Universidad del Rosario and
616 the University of Sheffield. The scanning electron microscope is funded via a EPSRC 4CU grant
617 (EP/K001329/1).

618

619 **References**

620 1. Silberglied RE, Taylor OR. Ultraviolet reflection and its behavioral role in the courtship of the
621 sulfur butterflies *Colias eurytheme* and *C. philodice* (Lepidoptera, Pieridae). Behav Ecol
622 Sociobiol. 1978;3: 203–243.

623 2. Obara Y, Ozawa G, Fukano Y, Watanabe K, Satoh T. Mate preference in males of the cabbage
624 butterfly, *Pieris rapae crucivora*, changes seasonally with the change in female UV color.
625 Zoolog Sci. 2008;25: 1–5.

626 3. Rutowski RL. The use of visual cues in sexual and species discrimination by males of the small
627 sulphur butterfly *Eurema lisa* (Lepidoptera, Pieridae). J Comp Physiol. 1977;115: 61–74.

628 4. Sweeney A, Jiggins C, Johnsen S. Insect communication: Polarized light as a butterfly mating
629 signal. Nature. 2003;423: 31–32.

630 5. Kemp DJ, Rutowski RL. Condition dependence, quantitative genetics, and the potential signal
631 content of iridescent ultraviolet butterfly coloration. Evolution. 2007;61: 168–183.

632 6. Ghiradella H. Light and color on the wing: structural colors in butterflies and moths. Appl Opt.
633 1991;30: 3492–3500.

634 7. Lloyd VJ, Nadeau NJ. The evolution of structural colour in butterflies. Curr Opin Genet Dev.
635 2021;69: 28–34.

636 8. Wasik BR, Liew SF, Lilien DA, Dinwiddie AJ, Noh H, Cao H, et al. Artificial selection for
637 structural color on butterfly wings and comparison with natural evolution. Proc Natl Acad Sci U
638 S A. 2014;111: 12109–12114.

639 9. Stavenga DG, Leertouwer HL, Wilts BD. Coloration principles of nymphaline butterflies - thin
640 films, melanin, ommochromes and wing scale stacking. J Exp Biol. 2014;217: 2171–2180.

641 10. Thayer RC, Allen FI, Patel NH. Structural color in *Junonia* butterflies evolves by tuning scale
642 lamina thickness. Elife. 2020;9. doi:10.7554/eLife.52187

643 11. Vukusic P, Sambles JR, Lawrence CR, Wootton RJ. Quantified interference and diffraction in
644 single *Morpho* butterfly scales. Proc R Soc Lond B Biol Sci. 1999;266: 1403–1411.

645 12. Ghiradella H. Development of ultraviolet-reflecting butterfly scales: How to make an
646 interference filter. J Morphol. 1974;142: 395–409.

647 13. Rutowski RL, Macedonia JM, Merry JW, Morehouse NI, Yturralde K, Taylor-Taft L et al.
648 Iridescent ultraviolet signal in the orange sulphur butterfly (*Colias eurytheme)*: spatial, temporal
649 and spectral properties. Biological J. Linnean Soc. 2007;90: 349-364.

650 14. Parnell AJ, Bradford JE, Curran EV, Washington AL, Adams G, Brien MN, et al. Wing scale
651 ultrastructure underlying convergent and divergent iridescent colours in mimetic butterflies. J R
652 Soc Interface. 2018;15. doi:10.1098/rsif.2017.0948

653 15. Davis AL, Nijhout HF, Johnsen S. Diverse nanostructures underlie thin ultra-black scales in
654 butterflies. Nat Commun. 2020;11: 1294.

655 16. Vukusic P, Sambles JR, Lawrence CR. Structurally assisted blackness in butterfly scales. Proc
656 Biol Sci. 2004;271 Suppl 4: S237–9.

657 17. Concha C, Wallbank RWR, Hanly JJ, Fenner J, Livraghi L, Rivera ES, et al. Interplay between
658 Developmental Flexibility and Determinism in the Evolution of Mimetic *Heliconius* Wing
659 Patterns. Curr Biol. 2019;29: 3996–4009.e4.

660 18. Zhang L, Mazo-Vargas A, Reed RD. Single master regulatory gene coordinates the evolution and
661 development of butterfly color and iridescence. Proc Natl Acad Sci U S A. 2017;114: 10707–
662 10712.

663 19. Matsuoka Y, Monteiro A. Melanin Pathway Genes Regulate Color and Morphology of Butterfly
664 Wing Scales. Cell Rep. 2018;24: 56–65.

665 20. Reed RD, Papa R, Martin A, Hines HM, Counterman BA, Pardo-Diaz C, et al. *optix* drives the
666 repeated convergent evolution of butterfly wing pattern mimicry. Science. 2011;333: 1137–1141.

667 21. Mallet J, Barton NH. Strong natural selection in a warning-color hybrid zone. Evolution.
668 1989;43: 421–431.

669 22. Nadeau NJ. Genes controlling mimetic colour pattern variation in butterflies. Curr Opin Insect
670 Sci. 2016;17: 24–31.

671 23. Brien MN, Enciso-Romero J, Parnell AJ, Salazar PA, Morochz C, Chalá D, et al. Phenotypic
672 variation in crosses shows that iridescent structural colour is sex-linked and controlled by
673 multiple genes. Interface Focus. 2019;9: 20180047.

674 24. Kozak KM, Wahlberg N, Neild AFE, Dasmahapatra KK, Mallet J, Jiggins CD. Multilocus
675 species trees show the recent adaptive radiation of the mimetic H*eliconius* butterflies. Syst Biol.
676 2015;64: 505–524.

677 25. Sheppard PM. Genetics and the evolution of Müllerian mimicry in *Heliconius* butterflies.
678 Philosophical Transactions of the Royal Society of London. B, Biological Sciences. 1985: 433–
679 610. doi:10.1098/rstb.1985.0066

680 26. Curran EV, Stankowski S, Pardo-Diaz C, Salazar C, Linares M, Nadeau NJ. Müllerian mimicry
681 of a quantitative trait despite contrasting levels of genomic divergence and selection. Mol Ecol.
682 2020;29: 2016–2030.

683 27. Manceau M, Domingues VS, Linnen CR, Rosenblum EB, Hoekstra HE. Convergence in
684 pigmentation at multiple levels: mutations, genes and function. Philosophical Transactions of the
685 Royal Society B: Biological Sciences. 2010. pp. 2439–2450. doi:10.1098/rstb.2010.0104

686 28. Hubbard JK, Uy JAC, Hauber ME, Hoekstra HE, Safran RJ. Vertebrate pigmentation: from
687 underlying genes to adaptive function. Trends Genet. 2010;26: 231–239.

688 29. Conte GL, Arnegard ME, Peichel CL, Schluter D. The probability of genetic parallelism and
689 convergence in natural populations. Proc Biol Sci. 2012;279: 5039–5047.

690 30. Wilts BD, Vey AJM, Briscoe AD, Stavenga DG. Longwing (*Heliconius*) butterflies combine a
691 restricted set of pigmentary and structural coloration mechanisms. BMC Evol Biol. 2017;17: 226.

692 31. Chen W-M, Abecasis GR. Family-based association tests for genome wide association scans. Am
693 J Hum Genet. 2007;81: 913–926.

694 32. Aulchenko YS, Ripke S, Isaacs A, van Duijn CM. GenABEL: an R library for genome-wide
695 association analysis. Bioinformatics. 2007;23: 1294–1296.

696 33. Thurmond J, Goodman JL, Strelets VB, Attrill H, Gramates LS, Marygold SJ, et al. FlyBase 2.0:
697 the next generation. Nucleic Acids Res. 2018;47: D759–D765.

698 34. Ferguson LC, Maroja L, Jiggins CD. Convergent, modular expression of ebony and tan in the
699 mimetic wing patterns of *Heliconius* butterflies. Dev Genes Evol. 2011;221: 297–308.

700 35. Gruson H, Andraud C, Daney de Marcillac W, Berthier S, Elias M, Gomez D. Quantitative
701 characterization of iridescent colours in biological studies: a novel method using optical theory.
702 Interface Focus. 2019;9: 20180049.

703 36. Kinoshita S, Yoshioka S. Structural colors in nature: the role of regularity and irregularity in the
704 structure. ChemPhysChem. 2005;6: 1442–1459.

705 37. Colosimo PF, Hosemann KE, Balabhadra S, Villarreal G Jr, Dickson M, Grimwood J, et al.
706 Widespread parallel evolution in sticklebacks by repeated fixation of Ectodysplasin alleles.
707 Science. 2005;307: 1928–1933.

708 38. Burke MK, Liti G, Long AD. Standing genetic variation drives repeatable experimental evolution
709 in outcrossing populations of *Saccharomyces cerevisiae*. Mol Biol Evol. 2014;31: 3228–3239.

710 39. Slate J. From beavis to beak color: a simulation study to examine how much QTL mapping can
711 reveal about the genetic architecture of quantitative traits. Evolution. 2013;67: 1251–1262.

712 40. Xu S. Theoretical Basis of the Beavis Effect. Genetics. 2003;165: 2259–2268.

713 41. Rice WR. Sex Chromosomes and the Evolution of Sexual Dimorphism. Evolution. 1984. p. 735.
714 doi:10.2307/2408385

715 42. Reinhold K. Sex linkage among genes controlling sexually selected traits. Behav Ecol Sociobiol.
716 1998;44: 1–7.

717 43. Brien MN. The genetics and evolution of iridescent structural colour in *Heliconius* butterflies.
718 PhD thesis, University of Sheffield. 2019.

719 44. Fenner J, Benson C, Rodriguez-Caro L, Ren A, Papa R, Martin A, et al. *Wnt* Genes in Wing
720 Pattern Development of Coliadinae Butterflies. Frontiers in Ecology and Evolution. 2020.
721 doi:10.3389/fevo.2020.00197

722 45. Livraghi L, Hanly JJ, Van Belleghem SM, Montejo-Kovacevich G, van der Heijden ESM, Loh
723 LS, et al. *Cortex cis*-regulatory switches establish scale colour identity and pattern diversity in
724 *Heliconius*. bioRxiv. 2021. doi:10.1101/2020.05.26.116533

725 46. Zhang L, Martin A, Perry MW, van der Burg KRL, Matsuoka Y, Monteiro A, et al. Genetic
726 Basis of Melanin Pigmentation in Butterfly Wings. Genetics. 2017. pp. 1537–1550.
727 doi:10.1534/genetics.116.196451

728 47. Bainbridge HE, Brien MN, Morochz C, Salazar PA, Rastas P, Nadeau NJ. Limited genetic
729 parallels underlie convergent evolution of quantitative pattern variation in mimetic butterflies. J
730 Evol Biol. 2020. doi:10.1111/jeb.13704

731 48. Baxter SW, Davey JW, Johnston JS, Shelton AM, Heckel DG, Jiggins CD, et al. Linkage
732 mapping and comparative genomics using next-generation RAD sequencing of a non-model
733 organism. PLoS One. 2011;6: e19315.

734 49. Van Belleghem SM, Rastas P, Papanicolaou A, Martin SH, Arias CF, Supple MA, et al.
735 Complex modular architecture around a simple toolkit of wing pattern genes. Nat Ecol Evol.
736 2017;1: 52.

737 50. Davey JW, Chouteau M, Barker SL, Maroja L, Baxter SW, Simpson F, et al. Major
738 Improvements to the *Heliconius melpomene* Genome Assembly Used to Confirm 10
739 Chromosome Fusion Events in 6 Million Years of Butterfly Evolution. G3. 2016;6: 695–708.

740 51. Langmead B, Salzberg SL. Fast gapped-read alignment with Bowtie 2. Nat Methods. 2012;9:
741 357–359.

742 52. Li H. A statistical framework for SNP calling, mutation discovery, association mapping and
743 population genetical parameter estimation from sequencing data. Bioinformatics. 2011;27: 2987–
744 2993.

745 53. Rastas P. Lep-MAP3: robust linkage mapping even for low-coverage whole genome sequencing
746 data. Bioinformatics. 2017;33: 3726–3732.

747 54. Morris J, Navarro N, Rastas P, Rawlins LD, Sammy J, Mallet J, et al. The genetic architecture of
748 adaptation: convergence and pleiotropy in *Heliconius* wing pattern evolution. Heredity.
749 2019;123: 138–152.

750 55. Vischer N. PeakFinder. 2013. Available:
751 https://sils.fnwi.uva.nl/bcb/objectj/examples/PeakFinder/PeakFinderTool.txt

752 56. Schindelin J, Arganda-Carreras I, Frise E, Kaynig V, Longair M, Pietzsch T, et al. Fiji: an open-
753 source platform for biological-image analysis. Nat Methods. 2012;9: 676–682.

754 57. Sivia DS. Elementary Scattering Theory: For X-ray and Neutron Users. OUP Oxford; 2011.

755 58. Kieffer J, Karkoulis D. PyFAI, a versatile library for azimuthal regrouping. J Phys Conf Ser.
756 2013;425: 202012.

757 59. Knudsen EB, Sørensen HO, Wright JP, Goret G, Kieffer J. FabIO: easy access to two-
758 dimensional X-ray detector images in Python. J Appl Crystallogr. 2013;46: 537–539.

759 60. Vincent T, Valls V, payno, Kieffer J, Solé VA, Paleo P, et al. silx-kit/silx: v0.13.0 beta 0:
760 21/02/2020. 2020. doi:10.5281/zenodo.3678538

761 61. Broman KW, Wu H, Sen S, Churchill GA. R/qtl: QTL mapping in experimental crosses.
762 Bioinformatics. 2003. pp. 889–890. doi:10.1093/bioinformatics/btg112

763 62. Broman KW, Gatti DM, Simecek P, Furlotte NA, Prins P, Sen Ś, et al. R/qtl2: Software for
764 Mapping Quantitative Trait Loci with High-Dimensional Data and Multiparent Populations.
765 Genetics. 2019. pp. 495–502. doi:10.1534/genetics.118.301595

766 63. Challis RJ, Kumar S, Dasmahapatra KK, Jiggins CD, Blaxter M. Lepbase: the Lepidopteran
767 genome database. 2016. doi:10.1101/056994

768 64. Altschul SF, Gish W, Miller W, Myers EW, Lipman DJ. Basic local alignment search tool. J Mol
769 Biol. 1990;215: 403–410.

770